

Fatigue crack growth mechanism in cast hybrid metal matrix composite reinforced with SiC particles and Al₂O₃ whiskers

AKM Asif IQBAL¹, Yoshio ARAI², Wakako ARAKI²

1. Graduate School of Science and Engineering, Saitama University, Saitama, Japan;
2. Division of Mechanical Engineering and Science, Graduate School of Science and Engineering, Saitama University, Saitama, Japan

Received 18 June 2013; accepted 25 November 2013

Abstract: The fatigue crack growth (FCG) mechanism of a cast hybrid metal matrix composite (MMC) reinforced with SiC particles and Al₂O₃ whiskers was investigated. For comparison, the FCG mechanisms of a cast MMC with Al₂O₃ whiskers and a cast Al alloy were also investigated. The results show that the FCG mechanism is observed in the near-threshold and stable-crack-growth regions. The hybrid MMC shows a higher threshold stress intensity factor range, ΔK_{th} , than the MMC with Al₂O₃ and Al alloy, indicating better resistance to crack growth in a lower stress intensity factor range, ΔK . In the near-threshold region with decreasing ΔK , the two composite materials exhibit similar FCG mechanism that is dominated by debonding of the reinforcement–matrix interface, and followed by void nucleation and coalescence in the Al matrix. At higher ΔK in the stable- or mid-crack-growth region, in addition to the debonding of the particle–matrix and whisker–matrix interface caused by cycle-by-cycle crack growth at the interface, the FCG is affected predominantly by striation formation in the Al matrix. Moreover, void nucleation and coalescence in the Al matrix and transgranular fracture of SiC particles and Al₂O₃ whiskers at high ΔK are also observed as the local unstable fracture mechanisms. However, the FCG of the monolithic Al alloy is dominated by void nucleation and coalescence at lower ΔK , whereas the FCG at higher ΔK is controlled mainly by striation formation in the Al grains, and followed by void nucleation and coalescence in the Si clusters.

Key words: cast metal matrix composites; fatigue crack growth; stress intensity factor ; fracture

1 Introduction

Discontinuously reinforced metal matrix composites (MMCs) have attracted extensive research interest in the past few decades owing to their high specific strength, and high wear resistance as compared with their corresponding monolithic alloys. Reinforcement using particulates generally results in isotropic mechanical properties, which have led to numerous structural applications for aluminium-based metal matrix composites (Al-MMC) in the automobile and aerospace industries [1].

A large number of systematic experimental studies have been conducted to determine the FCG responses of a variety of aluminium alloys reinforced with either SiC or Al₂O₃ particulates [2–9]. These studies concluded that, in general, composite materials had higher threshold values in the stress intensity factor range, ΔK_{th} , than their

monolithic materials. CHAWLA et al [10] observed that increasing volume fraction and decreasing particle size resulted in an increase in ΔK_{th} . Moreover, BOTSTEIN et al [11] found higher crack growth rates in the mid-growth rate (Paris law) region than monolithic alloys while doing experiments with Al2014–40%SiC_p and Al7091–30%SiC_p composites. Furthermore, SUGIMURA and SURESH [4] explained that large SiC particulate-reinforced composites demonstrated lower FCG performance with increased ΔK because of a particle fracture-dominated growth mechanism. In addition, several researchers have investigated the effect of particle clustering on FCG in Al-MMCs [11,12]. They determined that particle clustering significantly increased crack growth in the mid-growth rate (Paris law) region. It has been widely demonstrated that the FCG response of SiC particulate-reinforced composites strongly depended on the nature of the underlying interaction between the reinforcing particles and the advancing fatigue crack

front. Several studies have explained this interaction in terms of particle–matrix interfacial debonding [3,7], particle fracture [4,13], crack deflection around the reinforcing particles and subsequent FCG through the matrix [2,13,14], and particle crack trapping [15].

Many of the FCG studies described above were performed with either particulate- or whisker-reinforced MMCs, and a few investigations have been made recently in which the FCG behavior of hybrid reinforcements was investigated. For example, the effects of whiskers and particles on fatigue crack growth in SiC_p and SiC_w hybrid composites were compared by MASON and RITCHIE [16]. They observed that crack growth resistance in the composites was superior to that in a monolithic alloy at low stress intensity ranges, ΔK , owing to the formation of tortuous crack paths, which in turn enhanced roughness-induced crack closure. OH and HAN [17] pointed out that the increase in ΔK_{th} with increasing particle content in hybrid MMCs reinforced with Al₂O₃ short fibers and Al₂O₃ particles indicates that the crack growth resistance was enhanced over the entire ΔK , and thus hybrid-reinforced composites provide better control of damage tolerance properties over conventional particle-reinforced composites. However, the FCG behavior of cast hybrid MMCs reinforced with SiC particles and Al₂O₃ whiskers has not yet been investigated. The authors strongly believe that investigating the FCG mechanism of cast hybrid MMCs would provide a better understanding to use this material in large-scale structural applications, e.g., the brake disc of a high-speed railway coach.

In the present study, the FCG mechanism in the near-threshold region and mid-growth-rate (Paris law) region was thoroughly investigated in three different types of materials: cast hybrid MMC (SiC particles+ Al₂O₃ whiskers), cast MMC reinforced with Al₂O₃ whiskers, and unreinforced cast Al alloy. The experimental results are discussed in terms of a comparison of the observed mechanisms in the three materials.

2 Experimental

Three types of materials were used to investigate the fatigue crack growth mechanisms: cast aluminium alloy JIS-AC4CH [18], cast MMC with 9% Al₂O₃ whiskers as reinforcement, and cast hybrid MMC. The hybrid MMC was fabricated with 21% (volume fraction) SiC particles and 9% Al₂O₃ whiskers as reinforcements and the aluminium alloy JIS-AC4CH as the matrix. As reported previously [19], because of the formation process of the preforms, the whiskers in both MMCs were randomly oriented in a plane. In this article, “longitudinal cross section” is defined as the plane and

“lateral cross section” is defined as that perpendicular to the plane. The mechanical properties of reinforcement and tested materials are shown in Table 1. The listed properties for both MMCs are in the direction of the longitudinal cross section. Figure 1 illustrates the microstructures of the three materials in the lateral and the longitudinal cross sections. Most of the SiC particles in the hybrid MMC are rectangular with sharp corners (Figs. 1(a) and (b)) and most of the Al₂O₃ whiskers in both MMC materials are roller-shaped (Figs. 1(a)–(d)). The average length of the SiC particles is 23 μm . The average length of the Al₂O₃ whiskers is 35 μm in the hybrid MMC and 38 μm in the MMC with Al₂O₃ whiskers. The average diameter of the Al₂O₃ whiskers is 2 μm in both MMCs. In the Al alloy, the average grain size is found to be 48 μm . The Si particles in the Al alloy are round with an average diameter of 3 μm . In both MMC materials, clusters of SiC particles and Al₂O₃ whiskers are observed at frequent intervals, as indicated by the broken lines in Figs. 1(b) and (d), respectively. Clustering of Si is also observed in the Al alloy, as shown by the broken line in Fig. 1(f).

Table 1 Mechanical properties of reinforcement and tested materials

Parameter	Al ₂ O ₃	SiC	Al alloy AC4CH	Hybrid MMC	MMC with Al ₂ O ₃ whisker
Elastic modulus/GPa	380	450	70.0	142	104
Poisson ratio	0.27	0.20	0.33	0.28	0.29
Yield strength/MPa	–	–	131	166	141
Tensile strength/MPa	–	–	262	228	200
Tensile elongation/%	–	–	9.22	2.77	5.44

Fatigue crack growth experiments were carried out on rectangular bar single-edge notched specimens by conventional three-point bending tests in a Shimazu ServoPulser using a special bending fixture equipped with a 5 kN load cell. The specimen dimensions are as follows: length of 100 mm, thickness of 8 mm, width of 6 mm, and notch width of 0.5 mm. The specimens were prepared by polishing the machined surface of the specimens using a polishing machine with 15, 3, and 1 μm diamond particles sequentially until all scratches and surface machining marks were removed. The span distance was 60 mm. Tests were conducted under ΔK control mode with a constant stress ratio $R=0.1$ in sinusoidal loading in accordance with the guidelines in ASTM E647 [20]. A decreasing ΔK procedure was used to determine the threshold stress intensity. The stress

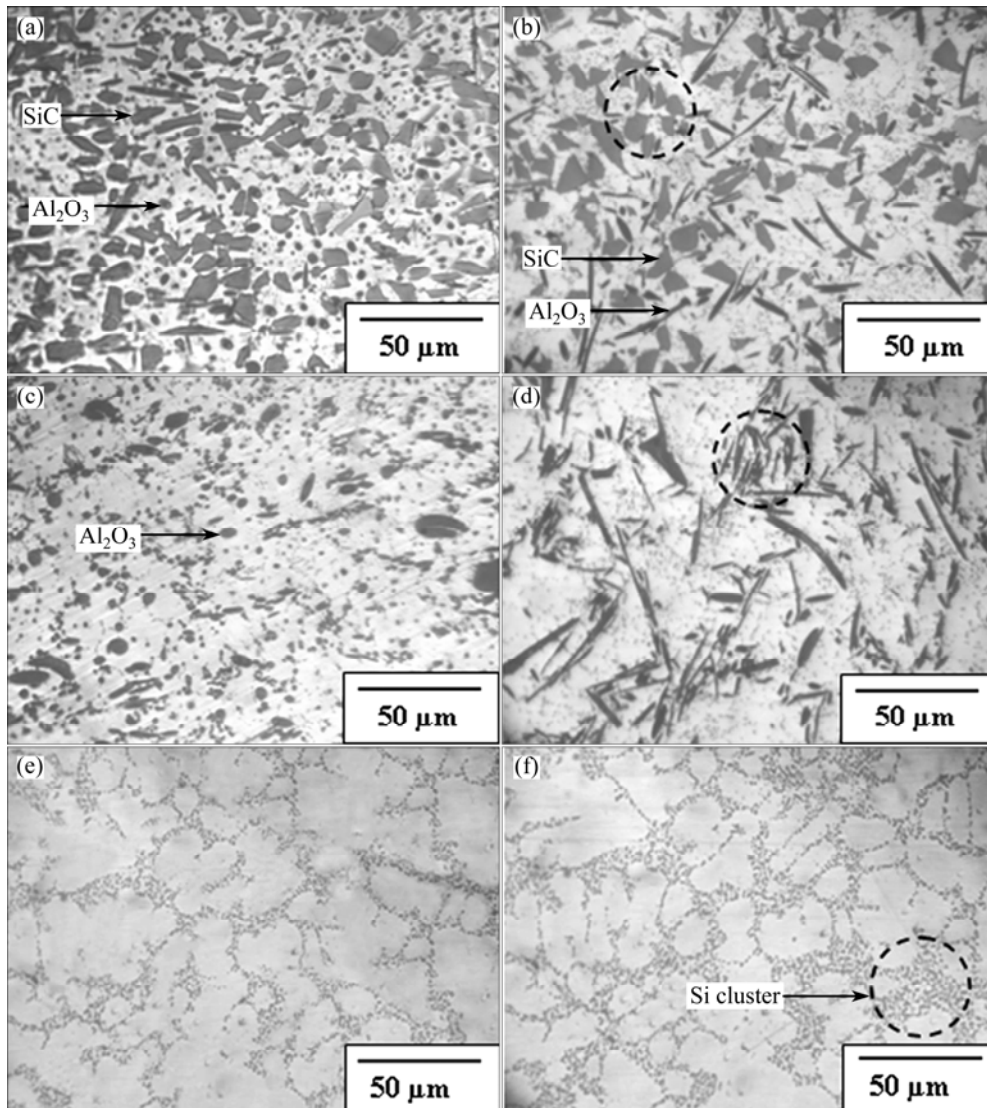


Fig. 1 Microstructures in lateral and longitudinal directions: (a), (b) Hybrid MMC; (c), (d) MMC with Al_2O_3 whiskers; (e), (f) Al alloy

intensity corresponding to a crack growth rate of 10^{-11} m/cycle was taken as the threshold stress intensity, ΔK_{th} . Once ΔK_{th} was determined, the crack growth was continued by increasing ΔK . Crack growth was measured using Bioten replicating films softened in acetone. The replicas were examined using an optical microscope. The tensile and fracture surfaces were comprehensively examined using scanning electron microscopy (SEM) and energy-dispersive X-ray spectroscopy (EDS), JEOL JSM-5600LV to characterize the near-threshold and stable- or mid-growth rate regions. Moreover, three-dimensional (3D) analysis was carried out to examine the roughness of the fracture surface using Mex software [21].

3 Results and discussion

Figure 2 demonstrates the fatigue crack growth characteristics for the hybrid MMC, MMC with Al_2O_3

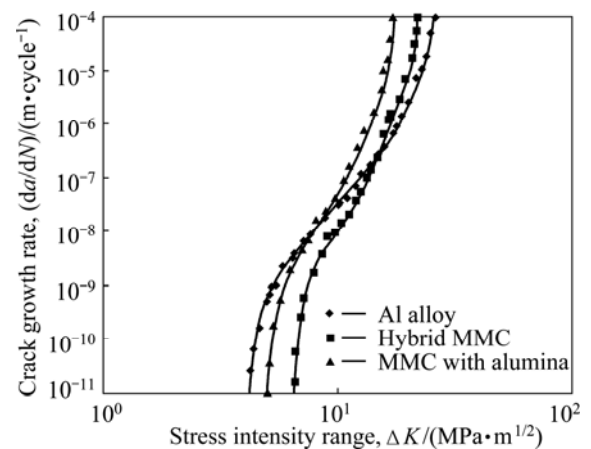


Fig. 2 Fatigue crack growth behaviour of hybrid MMC, MMC with Al_2O_3 whisker and Al alloy

whiskers, and Al alloy JIS-AC4CH under three regions: near threshold, stable crack growth, and rapid crack growth. The composite material reinforced with only

whiskers shows a higher crack growth rate (da/dN) than the monolithic alloy in the stable- and rapid-crack-growth regions. However, the hybrid MMC has a higher ΔK_{th} than the MMC with Al_2O_3 and the Al alloy, as summarized in Table 2. The higher value of ΔK_{th} for the hybrid MMC can be attributed to the higher modulus of the composite, which results in a lower crack-tip-opening displacement (CTOD) for a given applied ΔK . Treating the MMC as a homogeneous material, the CTOD of the three materials at threshold is calculated by using the Dugdale model assuming small-scale yielding [22] and the results are presented in Table 2. The results show that the hybrid MMC has the lowest crack-tip-opening displacement at the threshold stress intensity factor. The results are consistent with data in Refs. [23,24]. Furthermore, the two composites show higher values of the Paris-law exponent (m) than the unreinforced Al alloy, as presented in Table 2. The higher Paris-law slope

of the composites is thought to be due to lower fracture toughness of the composites relative to the unreinforced alloy. Moreover, the hybrid MMC exhibits better FCG resistance than the MMC with Al_2O_3 over the entire stress intensity range.

3.1 Hybrid MMC

Figures 3(a) and (c) illustrate the replica observation of FCG in the near-threshold and stable-crack-growth regions in the hybrid MMC. The horizontal arrows in the figures indicate the crack propagation direction. The value of da/dN is 1.64×10^{-11} m/cycle in the ΔK_{th} of 6.6 $MPa \cdot m^{1/2}$. Significant branching of the crack is seen near the crack tip in the threshold region (Fig. 3(a)). It has been reported that microstructural inhomogeneities such as inclusions, grain boundaries, and interfaces can generate crack kinking or branching, which cause significant retardation or even arrest of the subsequent crack propagation by reducing the crack driving force [24]. In the hybrid MMC, 21% (volume fraction) stiff SiC particles and 9% Al_2O_3 whiskers are present as inclusions, and thus the development of crack branching is significant, resulting in a reduction of the crack growth rate. Moreover, secondary microcracks with lengths of approximately 20–100 μm are observed ahead of the crack tip in both regions (indicated by arrows in Figs. 3(a) and (c)). These secondary microcracks form at the interface of the SiC particles and the Al matrix. It is evident from Figs. 3(a) and (c) that the number of secondary microcracks formed ahead of the crack tip in

Table 2 Fatigue crack growth test results and CTOD

Material	Fatigue threshold, $\Delta K_{th}/(MPa \cdot m^{1/2})$	Paris constant, C	Paris-law exponent, m	CTOD at threshold/ m
Hybrid MMC	6.6	8.7×10^{-15}	6	1.8×10^{-6}
MMC with Al_2O_3	5	2.2×10^{-14}	6.3	4×10^{-6}
Al alloy AC4CH	4.2	7.8×10^{-13}	4.5	1.9×10^{-6}

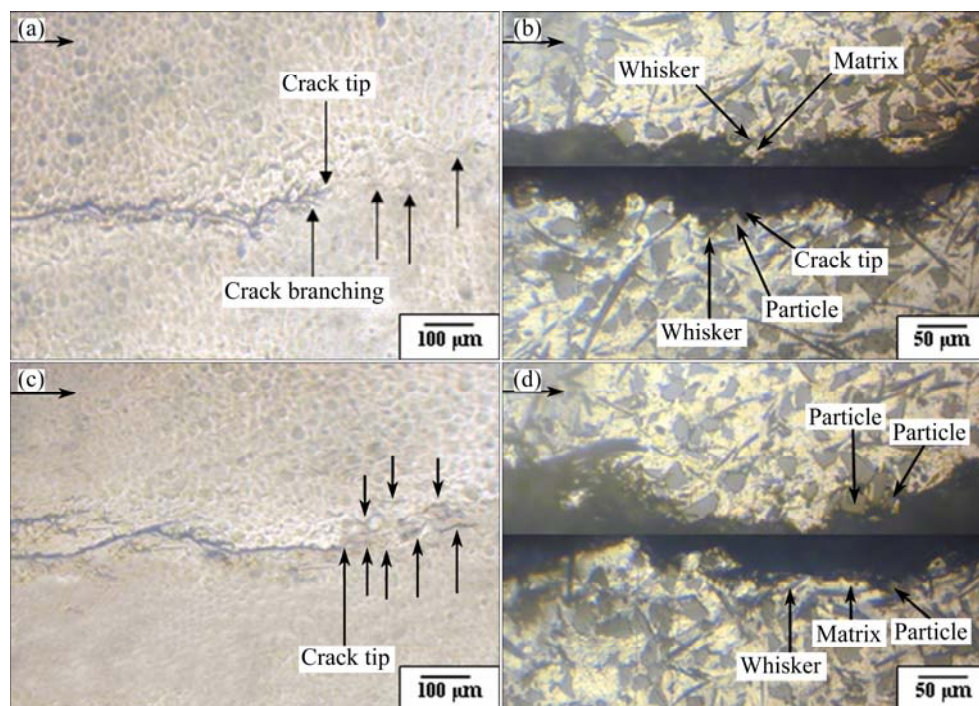


Fig. 3 Fatigue crack growth in hybrid MMC: (a), (c) Replica observation in near-threshold and stable-crack-growth regions; (b), (d) Matching tensile surface in near-threshold and stable-crack-growth regions

the stable-crack-growth region is reasonably higher than the microcracks formed in the threshold region in the hybrid MMC. Figures 3(b and (d) show optical micrographs of the near-threshold and stable-crack-growth regions, respectively, on the matching tensile surface of the fractured specimen. It is apparent that the threshold occurs at the cluster of SiC particles and Al₂O₃ whiskers, as shown in Fig. 3(b). No broken SiC particles are observed along the crack path in the near-threshold region (Fig. 3(b)), but partially broken particles are observed in the stable-crack-growth region (as indicated by the “Particle” and the “Whisker” arrows in Fig. 3(d)). Furthermore, the debonding of the SiC particles and Al matrix is frequently seen in both regions (as indicated by the “Particle” and the “Matrix” arrows in Figs. 3(b) and (d)). Once a crack meets a particle, it avoids the particle and detours round it.

Crack deflection around a particle is quite frequently seen regardless of ΔK value. During cyclic

loading, large strain mismatch occurs between the SiC particles and the Al matrix due to the elastic-plastic deformation mismatch and the stress becoming too high at the particle–matrix interface and cracks deflected round the particles. Moreover, many Al₂O₃ whiskers are found fractured or debonded from the Al matrix along the crack path in the near-threshold region as well as in the stable-crack-growth region. With planar random orientation of the whiskers, cracks meet the reinforcing whiskers either longitudinally or transversely. When a crack meets a longitudinal whisker, the whisker fractured ahead of the crack tip (as indicated by the “Whisker” and the “Whisker” arrows in Fig. 3(b)). The fracture mode resembles sectional-cut rather than pull-out, even though sometimes the corresponding ΔK is low. However, when a crack meets a whisker in the transverse direction, the whisker pulls the crack into the whisker–matrix interface and the successive interfacial separation occurs (indicated by “Whisker” arrows in Fig. 3(d)). Figure 4(a)

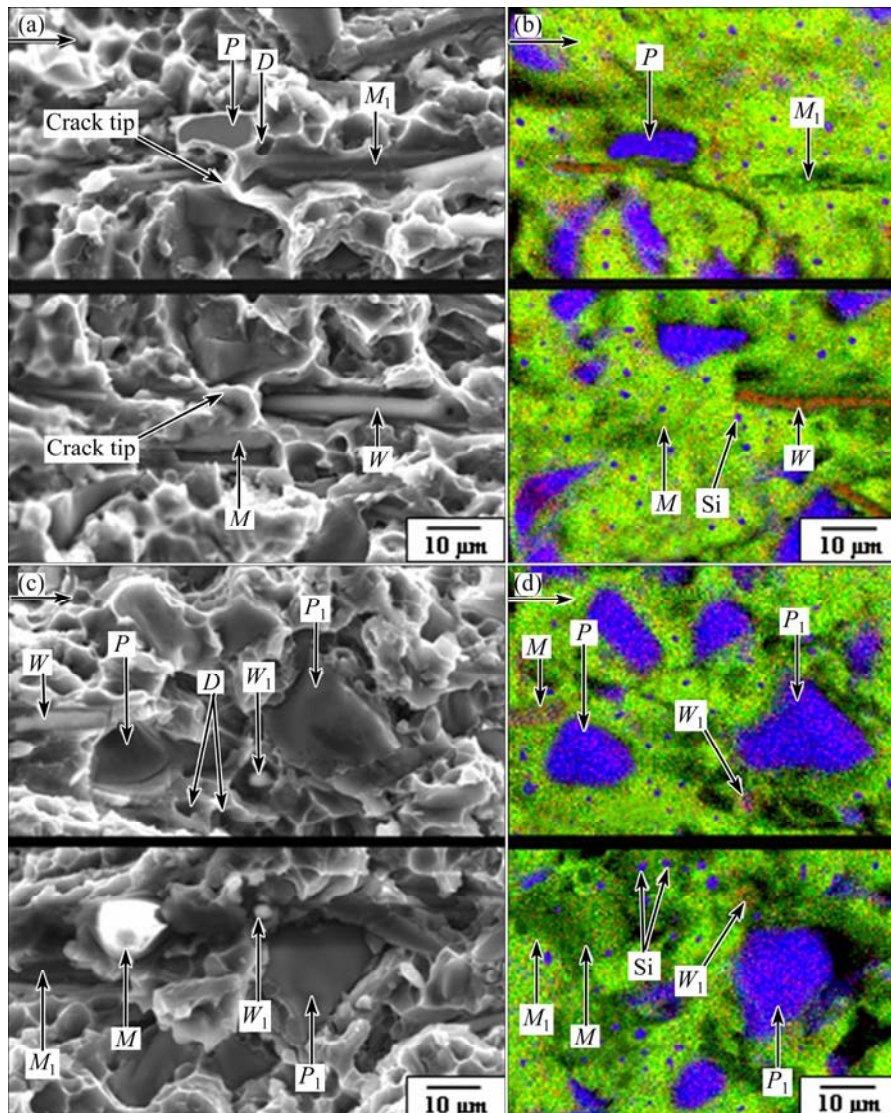


Fig. 4 Fatigue crack growth in hybrid MMC: (a), (c) SEM micrographs in near-threshold and stable-crack-growth regions; (b), (d) EDS analysis in near-threshold and stable-crack-growth regions

shows the SEM image of the matching fracture surface of the FCG in the near-threshold region. Figure 4(b) shows the EDS mapping analysis results of the areas corresponding to Fig. 4(a). The green, blue, and red colors in Fig. 4(b) indicate the presence of Al, Si, and O, respectively, on the fracture surfaces. In Fig. 4(b), the blue area indicated by P contains a significant amount of Si (96%) and a small amount of Al (4%), which identifies the area as a SiC particle (corresponding to P in Fig. 4(a)). The green area indicated by M contains a large amount of Al (95%) and a small amount of Si (5%), indicating that this area is the Al matrix (corresponding to M in Fig. 4(a)). Therefore, the blue and green areas indicated by the P – M pairs in the matching halves denote SiC particle–matrix interfacial debonding in the near-threshold region. Moreover, the red area (indicated by W in Fig. 4(b)) contains a large amount of Al (84%) and a small amount of O (16%), indicating the presence of an Al_2O_3 whisker (corresponding to W in Fig. 4(a)). The green area indicated by M_1 on the opposite side of the fracture surface indicates the Al matrix (Fig. 4(b)). Therefore, the W – M_1 pair in Fig. 4(b) (corresponding to the W – M_1 pair in Fig. 4(a)) denotes Al_2O_3 whisker–matrix interfacial debonding in the near-threshold region. Around the P – M and the W – M_1 pairs in Fig. 4(a), a number of dimples are nucleated (indicated by the D arrow in Fig. 4(a)) in the Al alloy matrix. EDS mapping analysis confirms the presence of a few Si particles on the opposite sides of the dimples. Dimple formation indicates the occurrence of void nucleation, which is induced by plastic deformation of the Al matrix around the second-phase Si particles. In addition, the SEM micrograph of the matching fracture surface of the FCG in the stable-crack-growth region and corresponding EDS mapping analysis results are presented in Figs. 4(c) and (d), respectively. Similar observation of particle–matrix interfacial debonding, whisker–matrix interfacial debonding, and void nucleation/coalescence in the Al matrix is found in this region. Moreover, the blue P_1 – P_1

pair and the red W_1 – W_1 pair in Fig. 4(d) indicate the presence of SiC particles and Al_2O_3 whiskers, respectively, on both sides of the fractured surface, meaning that interfacial debonding is followed by transgranular fracture in this crack-growth region (corresponding to the P_1 – P_1 pair and W_1 – W_1 pair in Fig. 4(c)). Furthermore, striation marks are observed in a few places in the stable-crack-growth region, as shown in Fig. 5(a). The average spacing of the striations is calculated to be $1.1\ \mu\text{m}$, which is very close to the da/dN value of $1\ \mu\text{m}/\text{cycle}$ at this stage. Moreover, the area fraction of the striations in the hybrid MMC in the stable-crack-growth region is calculated to be only 12.4%, as shown in Table 3. The EDS mapping analysis confirms that the striations form in the Al matrix (Fig. 5(b)). Because of the high plastic deformation of the Al matrix, the striation morphologies form in this crack-growth region during cyclic loading. However, the presence of Al_2O_3 whiskers and stiff SiC particles keeps the striation formation in a very limited area in the hybrid MMC. Figure 5(c) represents the 3D analysis of the striation. The top-to-top and bottom-to-bottom correspondence of the cyclic roughness indicates the wake of the crack-tip blunting and resharping.

Figure 6 demonstrates the 3D analysis of crack propagation from one SiC particle to another SiC particle in the near-threshold and stable-crack-growth regions. The crack surface profile of Fig. 6(b) clearly exhibits the existence of submicron roughness on the debonded particle–matrix interface. The edge of the dimple corresponds to the edge of the debonded interface, which means that the voids between the SiC–Al interfaces grow until they coalesce with the interfacial crack. However, the interfacial fracture between SiC-4 and Al alloy-4, indicated as a cross-sectional shape in Fig. 6(d), shows cyclic roughness, with an interval having the same order of magnitude as the crack growth rate. This means that the crack grows cycle by cycle at the interface, indicating that debonding take place over a number of cycles.

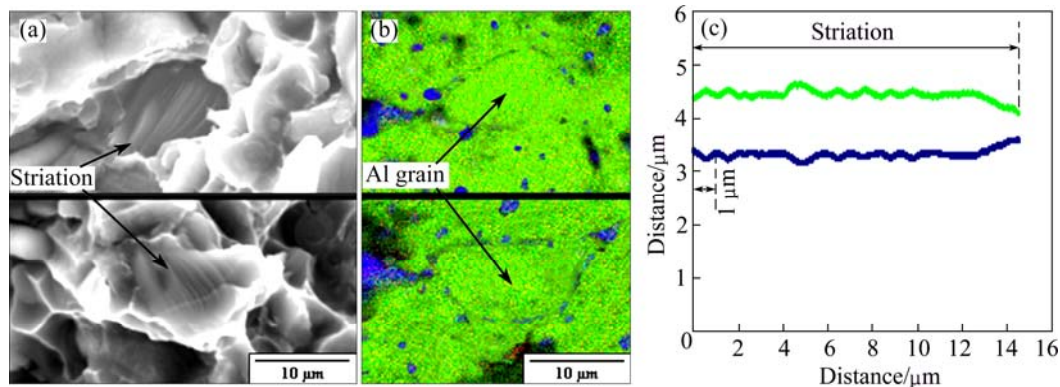


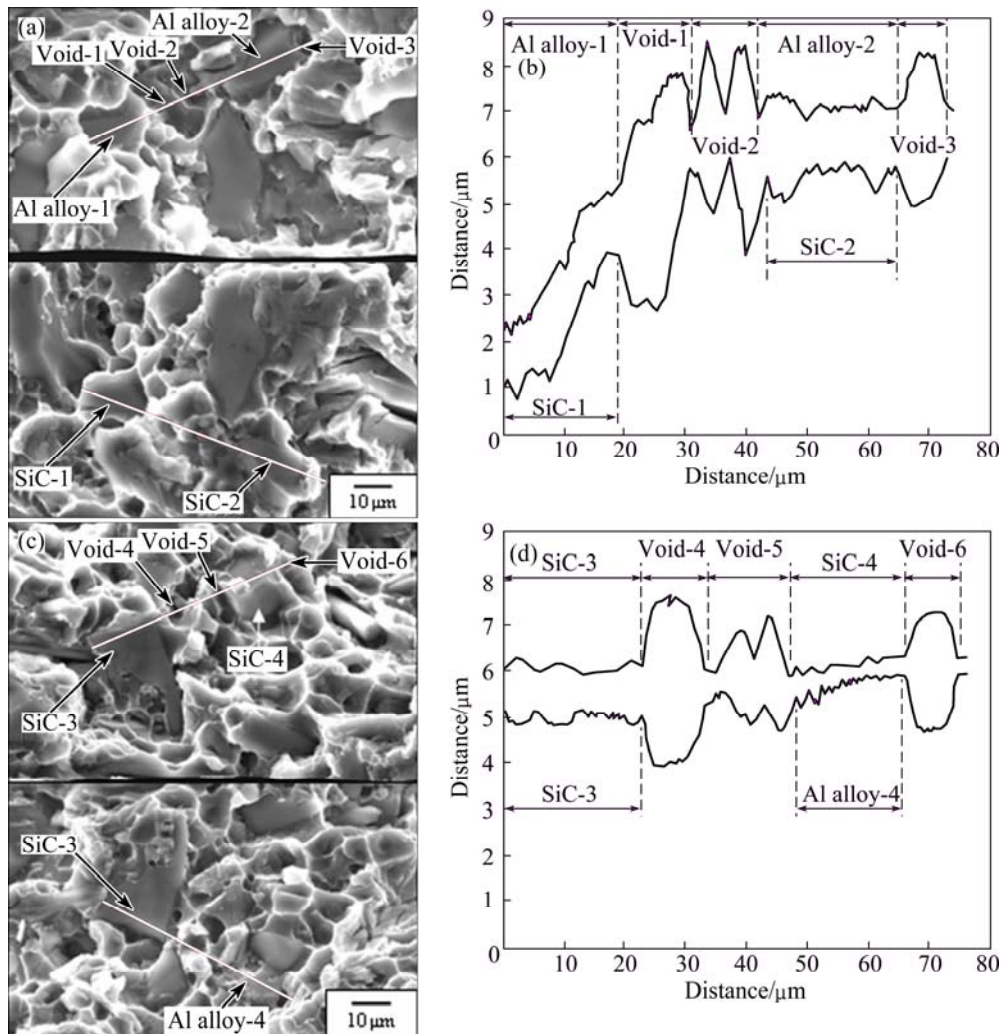
Fig. 5 Matching surface of striation formed in stable-crack-growth region of hybrid MMC: (a) SEM micrograph; (b) EDS mapping analysis; (c) 3D analysis

Table 3 Area fraction of striation in stable-crack-growth region of three materials (ΔK : Hybrid MMC, $16.4 \text{ MPa}\cdot\text{m}^{1/2}$; MMC with Al_2O_3 , $13 \text{ MPa}\cdot\text{m}^{1/2}$ and Al alloy, $18 \text{ MPa}\cdot\text{m}^{1/2}$)

Material	Hybrid MMC	MMC with Al_2O_3	Al alloy
Area fraction/%	12.4	41.5	76.3

The area fraction of SiC particle and Al_2O_3 whisker fracture and debonding between particle–matrix and whisker–matrix and the area fraction of dimples in the near-threshold and stable-crack-growth regions in hybrid MMC are presented in Table 4. The results indicate that interfacial debonding is the dominant mechanism of crack

growth in the near-threshold region, whereas particle fracture and whisker fracture play a vital role during crack growth in the mid-growth region. However, dimple formation is highly dominant in both regions. From the above observations, the FCG behavior of hybrid MMC is clearly perceived. In the near-threshold region, where the ΔK value is very low, the crack propagated by particle–matrix and whisker–matrix interfacial debonding is followed by void nucleation and coalescence. Further, with the higher ΔK values in the stable-crack-growth region, the crack propagated by the interfacial debonding of particle–matrix and whisker–matrix causes the cycle-by-cycle crack growth

**Fig. 6** 3D analysis of crack propagation from one SiC particle to another in hybrid MMC: (a), (c) Matching fracture surface in near-threshold and stable-crack-growth regions; (b), (d) Crack surface profile in near-threshold and stable-crack-growth regions**Table 4** Area fraction of SiC particle and Al_2O_3 whisker fracture and debonding between particle–matrix and whisker–matrix and area fraction of dimples of hybrid MMC in near-threshold region (ΔK : $6.6 \text{ MPa}\cdot\text{m}^{1/2}$) and stable-crack-growth region (ΔK : $16.4 \text{ MPa}\cdot\text{m}^{1/2}$)

Crack growth region	Area fraction of SiC Particle/%		Area fraction of Al_2O_3 whisker/%		Area fraction of dimple/%
	Fracture	Debonding	Fracture	Debonding	
Near-threshold	3.7	17.4	1.6	4.9	72.4
Stable-crack-growth	19.5	5.6	3.4	6.3	52.8

on the interface, as well as the transgranular fracture of particles and whiskers followed by striation formation and void nucleation in the Al alloy matrix.

3.2 MMC with Al₂O₃ whiskers

Figures 7(a) and (c) show the replica observation of FCG in the near-threshold and stable-crack-growth regions in the MMC with Al₂O₃ whiskers. It is seen on the specimen surface that the threshold occurs at the edge of a whisker angled toward the crack path. The value of da/dN is 1.02×10^{-11} m/cycle at ΔK_{th} of 5 MPa m^{1/2}. Because of the absence of interfacial fracture between the SiC particles and the Al matrix, the branching of cracks in the MMC with Al₂O₃ whiskers (indicated by arrow in Fig. 7(a)) is found to be less than that occurred in the hybrid MMC (indicated by arrow in Fig. 3(a)). Moreover, the number of secondary microcracks formed in the stable-crack-growth region of the MMC with Al₂O₃ whiskers is found to be reasonably less than that of the hybrid MMC. Figures 7(b) and (d) show the optical micrographs of the near-threshold and stable-crack-growth regions, respectively, of the matching tensile surface of the fractured specimen. The whisker shown in Fig. 7(a) is debonded from the matrix as the crack grows under ΔK that is relatively higher than the threshold value. Crack deflection is smaller in the MMC with Al₂O₃ than in the hybrid MMC.

Figures 8(a) and (b) illustrate the SEM micrograph and corresponding EDS mapping analysis results, respectively, of the matching fracture surface of the FCG in the near-threshold region. The vertical dotted lines in

Figs. 8(a) and (b) indicate the locations where the threshold occurs. The observed Al₂O₃ whisker–matrix interfacial debonding ($W-M$ pair) and whisker fracture (W_1-W_1 pair) are similar to that in the hybrid MMC in the near-threshold and the stable-crack-growth regions. A few dimples originate in the near-threshold region (indicated by D arrow in Fig. 8(a)) in the Al alloy matrix but the edges are indistinct. Al₂O₃ whiskers (W and W_1 in Figs. 8(a) and (b)) are present ahead of the crack tip when the threshold is reached, which indicates that the crack is arrested when it meets Al₂O₃ whiskers at the inner part of the specimen. Significant numbers of striation marks are observed in the stable-crack-growth region (indicated by the “Striation” arrows in Fig. 8(c)). The area fraction of the striations in the MMC with Al₂O₃ in the stable-crack-growth region is calculated to be 41.5%, as shown in Table 3. The EDS mapping analysis confirms that the striations form at the Al matrix. Because of the presence of only 9% of Al₂O₃ whiskers as reinforcement, the inter-reinforcement spacing in the MMC with Al₂O₃ whiskers is reasonably large and relatively large Al grains are present as compared with hybrid MMC. Formation of a multiple slip system is available because of the large Al grains. Thus, striation morphologies are formed over a relatively larger area in the MMC with Al₂O₃ whiskers as compared with the hybrid MMC. These results indicate that at lower ΔK values, fatigue crack growth is controlled by debonding of the whisker–matrix interface and void nucleation and coalescence in the Al alloy matrix. However, at higher ΔK values, FCG is controlled by debonding of the

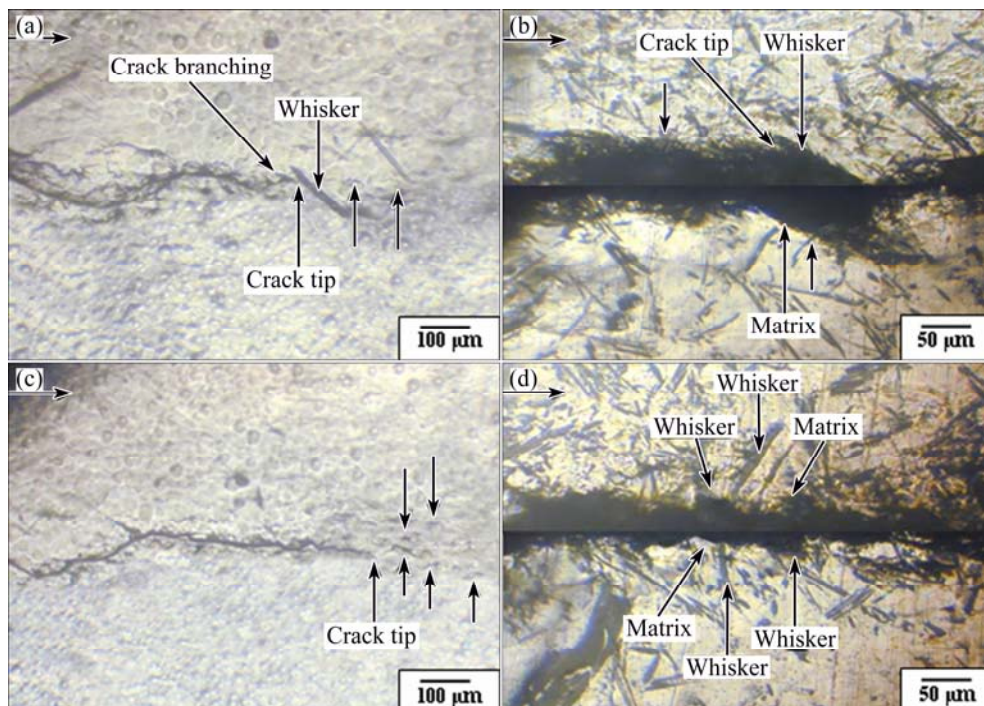


Fig. 7 Fatigue crack growth in MMC with Al₂O₃ whisker: (a), (c) Replica observation in near-threshold and stable-crack-growth regions; (b), (d) Matching tensile surface in near-threshold and stable-crack-growth regions

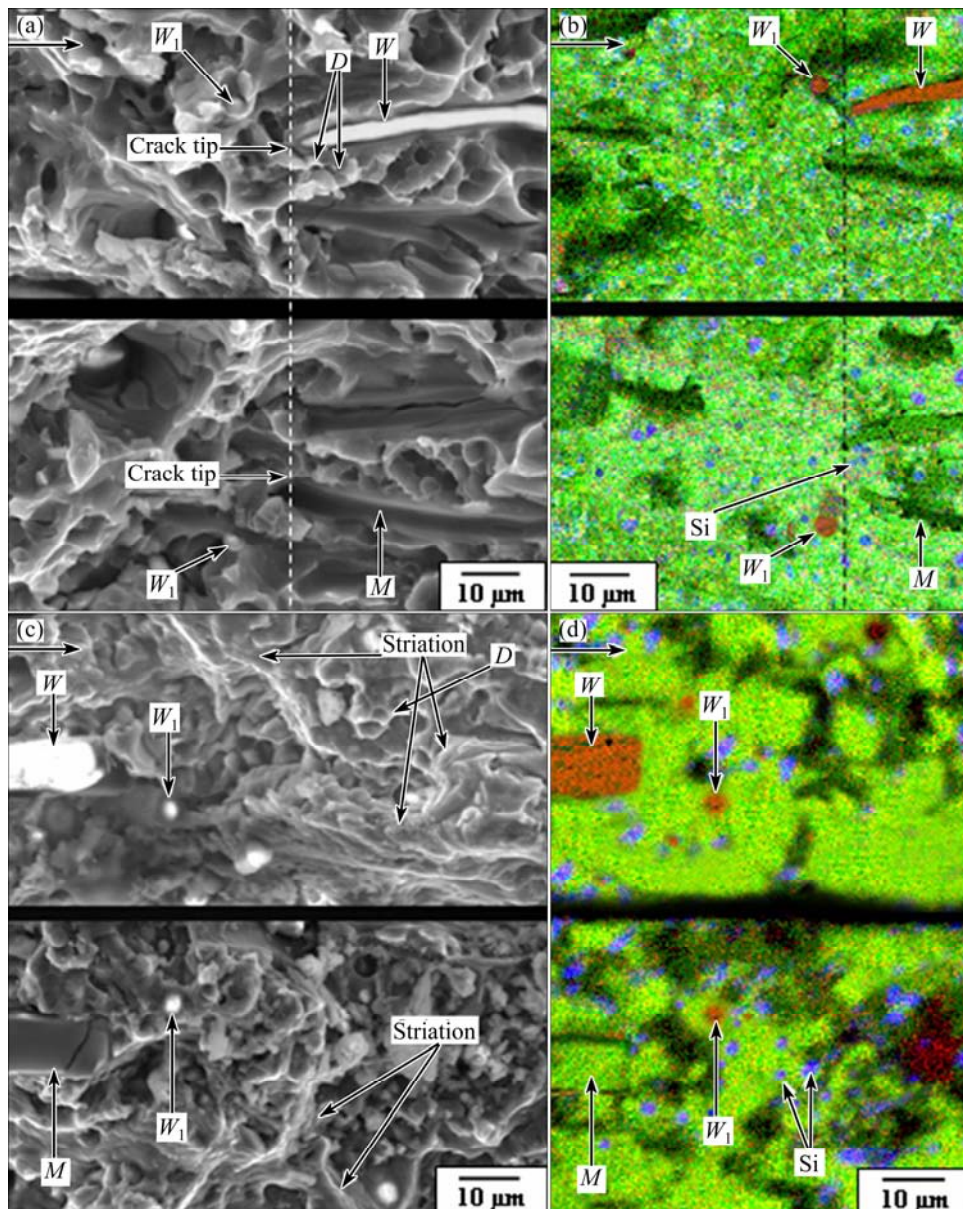


Fig. 8 Fatigue crack growth in MMC with Al_2O_3 whisker: (a), (c) SEM observation in near-threshold and stable-crack-growth regions; (b), (d) EDS analysis in near-threshold and stable-crack-growth regions

interface as well as whisker fracture followed by striation formation and void nucleation in the Al matrix.

3.3 Al alloy

The replica observation and the corresponding surface of FCG in the threshold region of the Al alloy are shown in Figs. 9(a) and (b), respectively. It is obvious from Fig. 9(b) that the fatigue threshold occurs at the cluster of Si particles on the specimen surface. The value of da/dN is 2.72×10^{-11} m/cycle when the value of ΔK_{th} is $4.2 \text{ MPa m}^{1/2}$. Moreover, Figs. 9(c) and (d) represent the replica observation and optical micrograph, respectively, of the Al alloy in the stable-crack-growth region. It is observed that the crack moves along the boundary between the Si particle cluster and the Al grains on the

specimen surface. Crack branching and secondary microcracks are found very less near the crack tip in the near-threshold and stable-crack-growth regions (Figs. 9(a) and (c)) in comparison with the hybrid MMC and the MMC with Al_2O_3 whiskers. In the Al alloy, only Si particles with $3 \mu\text{m}$ in diameter are present as inclusions. Therefore, the microstructural homogeneity of this material is higher than those of the other two composite materials, and limited crack branching is seen during FCG. Figure 10(a) shows the SEM micrograph of the matching fracture surface of the Al alloy in the near-threshold region, showing a relatively smooth surface with dimples. In the EDS mapping in Fig. 10(b), Si particles are observed on the fracture surface, which means that the crack has reached its threshold at the Si

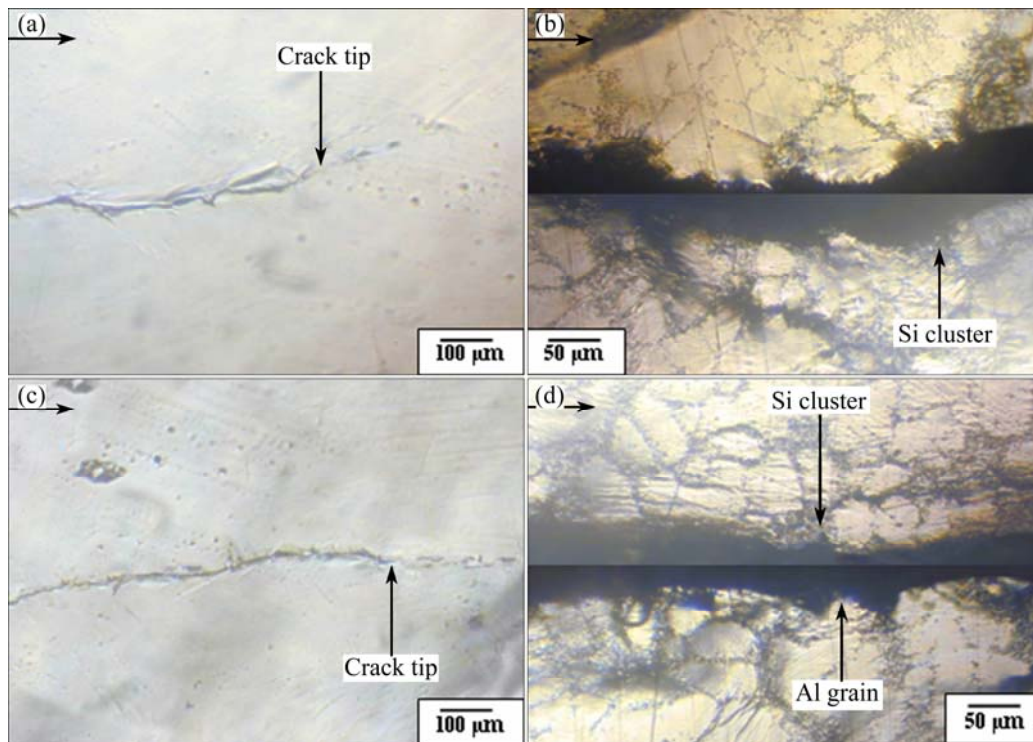


Fig. 9 Fatigue crack growth in Al alloy: (a), (c) Replica observation in near-threshold and stable-crack-growth regions; (b), (d) Matching tensile surface in near-threshold and stable-crack-growth regions

particle cluster at the inner side of the specimen. Moreover, Figs. 10(c) and (d) represent the fracture surface and the corresponding EDS analysis results, respectively, in the stable-crack-growth region. Numerous striation marks are observed on this fracture surface along the crack propagation path. The average spacing of the striations is calculated to be 1 μm , which is close to the value of da/dN at this stage. The area fraction of the striations in this region is calculated to be 76.3%, as shown in Table 3. The large green areas in Fig. 10(d) confirm the presence of Al grains where the striations form. In the stable-crack-growth region, multiple slip systems are in operation because of the presence of large Al grains. Consequently, striation morphologies form in large Al grains along the crack propagation path during cyclic loading. Moreover, in the stable-crack-growth region, the number of dimples is limited in the cluster of Si particles (indicated by arrows in Fig. 10(c)).

Figure 11 illustrates the FCG mechanism of the hybrid MMC, MMC with Al_2O_3 whiskers, and Al alloy in two different crack growth regions. The figure shows that the fatigue crack growth mechanisms in the two different regions of three different materials are strikingly different. Figures 11(a), (c), and (e) illustrate the crack growth mechanism in the near-threshold region of the three materials. It appears that reinforcement debonding is the dominant mechanism of crack growth

in the near-threshold region for both composite materials. The fatigue threshold ΔK_{th} and crack growth in the near-threshold region is previously explained in terms of crack closure [25]. It has been reported that several variables, including crack surface roughness, yield strength, and elastic modulus can influence crack closure and the value of the fatigue threshold ΔK_{th} [25,26]. Because the hybrid MMC contains SiC particles and Al_2O_3 whiskers, the modulus mismatch occurs between the particles, whiskers, and matrix. From the 3D analysis (Figs. 6(a) and (b)), the fracture of interface between the SiC particles and the Al alloy matrix is very frequently seen in the near-threshold region of hybrid MMCs, which leads to an increase in surface roughness as compared with the other two materials. Consequently, the fatigue threshold ΔK_{th} in the hybrid MMC increases. Furthermore, the elastic modulus and yield strength are also two important variables that can influence crack closure. It has been stated that a high modulus promotes crack closure [27]. In the mechanical properties set out in Table 1, the elastic modulus of the hybrid MMC is higher than that of the other two materials. Therefore, the crack growth resistance of the hybrid MMC is higher and the fatigue threshold increases. Figures 11(b), (d), and (f) illustrate the crack growth mechanisms in the stable- or mid-crack-growth regions of the three materials. Particle and whisker debonding from the matrix caused by the

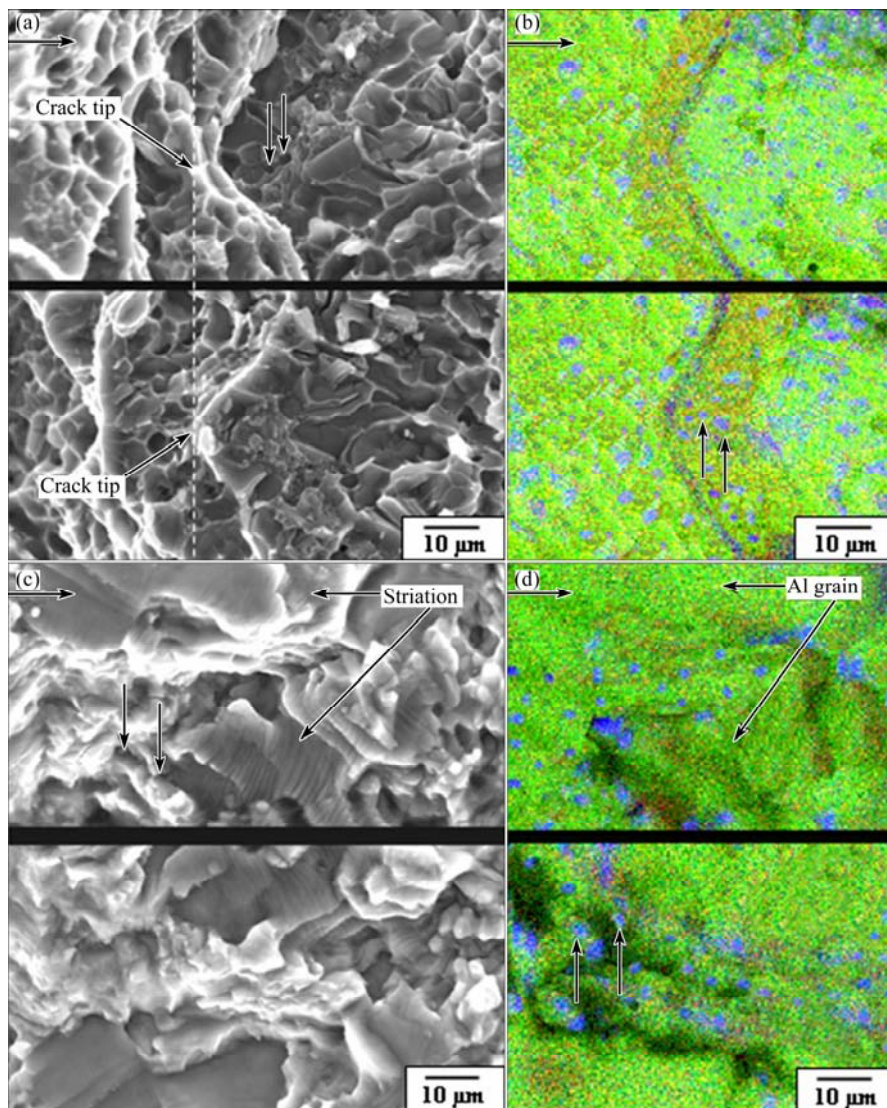


Fig. 10 Fatigue crack growth in Al alloy: (a), (c) SEM observation in near-threshold and stable-crack-growth regions; (b), (d) EDS analysis in near-threshold and stable-crack-growth regions

cycle-by-cycle crack growth at the interface and particle fractures in the hybrid MMC are frequently seen in this region. It has been stated that when the plastic zone is much larger than the size of the particles, the particle fracture may take place. Inserting the reinforcing particles and whiskers reduces the striation formation owing to the fracture of the reinforcing materials. The reduction of striation formation thus increases the crack propagation rate in the two MMCs.

4 Conclusions

1) The presence of SiC particles and Al₂O₃ whiskers in very close proximity facilitates the microstructural inhomogeneity of the cast hybrid MMC. In the low ΔK region, the SiC particles either act as barriers to cracks and or deflect the growth planes of cracks. In addition to

the high elastic modulus, crack deflection gives the cast hybrid MMC better fatigue crack growth resistance than the cast MMC with Al₂O₃ whisker and the cast Al alloy in the low ΔK region.

2) The FCG mechanisms of both MMC materials at decreasing ΔK in the near-threshold region are found to be quite similar. For both materials, FCG is dominated by the debonding of particle–matrix and whisker–matrix interfaces, and followed by void nucleation in the Al alloy matrix. The FCG reaches its threshold when the crack encounters the inhomogeneous distribution of the reinforcement or second-phase particles, i.e., the cluster of SiC particles and Al₂O₃ whiskers in the cast hybrid MMC, the Al₂O₃ whiskers in the cast MMC with Al₂O₃, and the cluster of Si particles in the cast Al alloy.

3) The FCG mechanism of both MMCs with increasing ΔK value in the stable- or mid-crack-growth

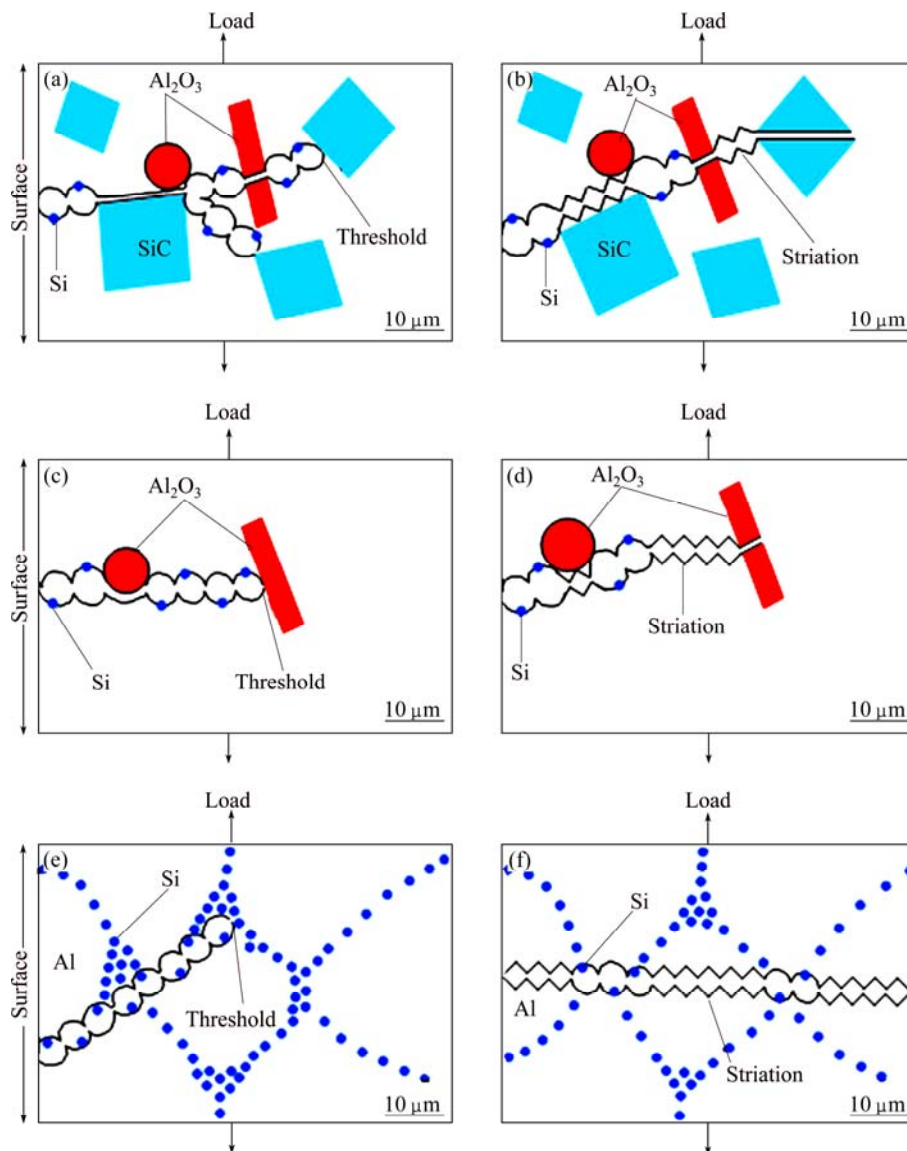


Fig. 11 Schematic diagrams of fatigue crack growth mechanism in near-threshold and stable-crack-growth regions: (a), (b) Hybrid MMC; (c), (d) MMC with Al_2O_3 whisker; (e), (f) Al alloy

region is the cycle-by-cycle crack growth along the particle–matrix and whisker–matrix interface, as well as the transgranular fracture of particles and whiskers. In addition, striation formation and void nucleation in the Al alloy matrix become the influential factors of crack growth in this region. Moreover, in the Al alloy, the FCG during higher ΔK values is controlled mainly by the striation formation in the large Al grains, and followed by the void nucleation and coalescence in the Si cluster.

Acknowledgement

The authors express gratitude to the Ministry of Education, Science, Sports and Culture of the Government of Japan for providing financial support during this research work.

References

- [1] MIRACLE D B. Metal matrix composites–From science to technological significance [J]. *Composite Science and Technology*, 2005, 65: 2526–2540.
- [2] DAVIDSON D L. Effect of particulate SiC on fatigue crack growth in a cast extruded aluminum alloy composite [J]. *Metallurgical Transaction A*, 1991, 22: 97–112.
- [3] KUMAI S, KING J E, KNOTT J F. Fatigue crack growth behavior in molten-metal processed SiC particle-reinforced aluminum alloys [J]. *Fatigue and Fracture of Engineering Materials and Structure*, 1992, 15: 1–11.
- [4] SUGIMURA Y, SURESH S. Effects of SiC content of fatigue crack growth in aluminum alloys reinforced with SiC particles [J]. *Metallurgical Transaction A*, 1992, 23: 2231–2242.
- [5] CHAWLA N, GANESH V V. Fatigue crack growth of SiC particle reinforced metal matrix composites [J]. *International Journal of Fatigue*, 2010, 32: 856–863.

- [6] CHEN Z Z, TOKAJI K. Effects of particle size on fatigue crack initiation and small crack growth in SiC particulate reinforced aluminium alloy composites [J]. *Materials Letters*, 2004, 58: 2314–2321.
- [7] WANG Z, ZHANG R J. Microscopic characteristics of fatigue crack propagation in aluminum alloy based particulate reinforced metal matrix composites [J]. *Acta Metallurgica et Materialia*, 1994, 42: 1433–1445.
- [8] LIU G, SHANG J K. Fatigue crack tip opening behavior in particulate reinforced Al alloy composites [J]. *Acta Metallurgica et Materialia*, 1996, 44: 79–91.
- [9] CRAWFORD B R, GRIFFITHS J R. Role of reinforcement particles during fatigue cracking of a micral-20-reinforced 6061 alloy [J]. *Fatigue and Fracture of Engineering Materials and Structure*, 1999, 22: 811–820.
- [10] CHAWLA N, ADRES C, JONES J W, ALLISON J E. Effect of SiC volume fraction and particle size on the fatigue resistance of a 2080 Al/SiC_p composite [J]. *Metallurgical and Materials Transactions A*, 1998, 29: 2843–2854.
- [11] BOTSTEIN O, ARONE R, SHPIGLER B. Fatigue crack growth mechanisms in Al–SiC particulate metal matrix composites [J]. *Materials Science and Engineering A*, 1990, 128: 15–22.
- [12] KNOWLES D M, KING J E. The influence of ageing on fatigue crack growth in SiC particulate reinforced 8090 Al alloy [J]. *Acta Metallurgica et Materialia*, 1991, 39: 793–806.
- [13] KUMAI S, YOSHIDA K, HIGO Y, NUNOMURA S. Effects of the particle distribution on fatigue crack growth in particulate SiC/6061 aluminum alloy composites [J]. *International Journal of Fatigue*, 1992, 14: 105–112.
- [14] DAVIDSON D L. The growth of fatigue cracks through particulate SiC reinforced aluminum alloys [J]. *Engineering Fracture Mechanics*, 1989, 33: 965–977.
- [15] SHANG J K, RITCHIE R O. On the particle-size dependence of fatigue-crack propagation thresholds in SiC-particulate-reinforced aluminum-alloy composites: Role of crack closure and crack trapping [J]. *Acta Metallurgica*, 1989, 37: 2267–2278.
- [16] MASON J J, RITCHIE R O. Fatigue crack growth resistance in SiC particulate and whisker reinforced P/M 2124 aluminum matrix composites [J]. *Materials Science and Engineering A*, 1997, 231: 170–182.
- [17] OH K H, HAN K S. Short-fiber/particle hybrid reinforcement: Effects on fracture toughness and fatigue crack growth of metal matrix composites [J]. *Composite Science and Technology*, 2007, 67: 1719–1726.
- [18] ‘Aluminium alloy castings’, JIS H5202 [S]. *Japan Industrial Standard*, 2002.
- [19] RAFIQUZZAMAN M D, ARAI Y. Hybrid effect on whisker orientation dependence of composite strength of aluminum cast alloy reinforced by Al₂O₃ whiskers and SiC particles [J]. *Journal of Solid Mechanics and Materials Engineering*, 2010, 4: 303–314.
- [20] E647-08 [S]. *ASTM Standard*, 2010.
- [21] Mex 5.1 [M]. *Alicona Imaging GmbH*.
- [22] ANDERSON T L. *Fracture mechanics: Fundamentals and applications* [M]. *CRC Press*, 1995.
- [23] LLORCA J. Fatigue of particle and whisker-reinforced metal matrix composites [J]. *Progress in Materials Science*, 2002, 47: 283–353.
- [24] BONEN J J, ALLISON J E, JONES J W. Fatigue behaviour of a 2xxx series aluminium alloy reinforced with 15 vol% SiC_p [J]. *Metallurgical Transaction A*, 1991, 22: 1007–1019.
- [25] MEGGIOLAROA M A, MIRANDAB A C O, CASTROA J T P, MARTHAC L F. Crack retardation equations for the propagation of branched fatigue cracks [J]. *International Journal of Fatigue*, 2005, 27: 1398–1407.
- [26] LAWSON L, CHEN E Y, MESHII M. Near threshold fatigue: A review [J]. *International Journal of Fatigue*, 1999, 21: 15–34.
- [27] WASEN J, HEIER E. Fatigue crack growth thresholds—The influence of Young's modulus and fracture roughness [J]. *International Journal of Fatigue*, 1988, 20: 737–742.

SiC_p 及 Al₂O_{3w} 增强铸态混杂金属基复合材料的疲劳裂纹扩展机理

AKM Asif IQBAL¹, Yoshio ARAI², Wakako ARAKI²

1. Graduate School of Science and Engineering, Saitama University, Saitama, Japan;

2. Division of Mechanical Engineering and Science, Graduate School of Science and Engineering, Saitama University, Saitama, Japan

摘要: 研究了一种 SiC_p 及 Al₂O_{3w} 增强铸态混杂金属基复合材料(MMC)的疲劳裂纹扩展 (FCG) 机理, 同时对比研究了 Al₂O_{3w} 增强铸态金属基复合材料和铸态铝合金的疲劳裂纹扩展机理。在研究近临界和裂纹稳定扩展区域的疲劳裂纹扩展 (FCG) 机理时, 发现混杂 MMC 的临界应力强度因子 ΔK_{th} 值高于其他两种材料的 ΔK_{th} 值, 说明应力强度因子 ΔK 值较低时混杂 MMC 可以更好地抵抗裂纹扩展。随着 ΔK 值的降低, 两种 MMC 在近临界区域显示出相似的 FCG 机理, 即主要由增强相-基体界面的剥离控制, 随后由铝基体中空隙的形核与合并控制; 在裂纹稳定或中等扩展区域, ΔK 值较高时 FCG 除了受界面上周期性裂纹扩展引起的增强相-基体界面剥离的影响之外, 还显著受到铝基体中疲劳条带的影响。此外, 在高 ΔK 值下, 因为局部失稳断裂机制, 可见铝基体中空隙的形核与合并以及 SiC_p 和 Al₂O_{3w} 中的穿晶断裂。对于铸态铝合金, 在低 ΔK 值下, FCG 主要受空隙的形核与合并所控制; 在高 ΔK 值下, FCG 主要受铝晶粒的疲劳条带控制, 随后受 Si 团簇中空隙的形核与合并控制。

关键词: 铸态金属基复合材料; 疲劳裂纹扩展; 应力强度因子; 断裂

(Edited by Xue-feng HE)